The conserved metalloprotease invadolysin localizes to the surface of lipid droplets

Neville Cobbe[1], Kathryn M. Marshall[2], Shubha Gururaja Rao[3], Ching-Wen Chang[1], Francesca Di Cara[1], Edward Duca[1], Sharron Vass[1], Adam Kassan[4] and Margarete M. S. Heck[1,*]

[1]University of Edinburgh, Queen's Medical Research Institute, Centre for Cardiovascular Science, 47 Little France Crescent, Edinburgh EH16 4TJ, UK
[2]Department of Surgery, University of Melbourne, Austin Health, Studley Road, Heidelberg, Melbourne, Victoria 3084, Australia
[3]Department of Molecular, Cell and Developmental Biology, University of California Los Angeles, Los Angeles, CA 90095, USA
[4]Departament de Biologia Cellular, Facultat de Medicina, Institut d'Investigacions Biomèdiques August Pi i Sunyer (IDIBAPS), Universitat de Barcelona, Casanova 143, 08036 Barcelona, Spain
*Author for correspondence (margarete.heck@ed.ac.uk)

Accepted 25 June 2009
Journal of Cell Science 122, 3414-3423 Published by The Company of Biologists 2009
doi:10.1242/jcs.044610

Summary

Invadolysin is a metalloprotease conserved in many different organisms, previously shown to be essential in *Drosophila* with roles in cell division and cell migration. The gene seems to be ubiquitously expressed and four distinct splice variants have been identified in human cells but not in most other species examined. Immunofluorescent detection of human invadolysin in cultured cells reveals the protein to be associated with the surface of lipid droplets. By means of subcellular fractionation, we have independently confirmed the association of invadolysin with lipid droplets. We thus identify invadolysin as the first metalloprotease located on these dynamic organelles. In addition, analysis of larval fat-body morphological appearance and triglyceride levels in the *Drosophila* invadolysin mutant suggests that invadolysin plays a role in lipid storage or metabolism.

Supplementary material available online at
http://jcs.biologists.org/cgi/content/full/122/18/3414/DC1

Key words: Invadolysin, Lipid droplets, Metalloprotease, Phylogeny

Introduction

A vast array of crucial metabolic functions are known to be regulated by highly specific proteolysis, allowing precise molecular control of diverse processes ranging from DNA replication and cell cycle progression to wound healing and angiogenesis (López-Otín and Overall, 2002). Many physiologically active proteins, such as enzymes or hormones, are often synthesized as inactive zymogen precursors that are subsequently activated by selective cleavage of peptide bonds, permitting amplification of small stimuli through a cascade (Neurath and Walsh, 1976). Proteases can thus play pivotal roles in both the generation and termination of various biological functions.

Invadolysin is a member of the M8 family of metzincin metalloproteases (Gomis-Rüth, 2003), the study of which has hitherto focused primarily on protozoan parasites responsible for diseases that cause high morbidity and mortality in developing countries (such as leishmaniasis and sleeping sickness). The best characterised of these proteins is leishmanolysin from *Leishmania major*, otherwise known as gp63 (Yao et al., 2003), which is believed to play an important role in the virulence of *Leishmania*. Larvae of *Drosophila* homozygous for the original *invadolysin* mutant allele (termed *IX-14*) die in the late larval stages, with aberrant mitotic phenotypes clearly discernible in neuroblasts (McHugh et al., 2004). Other phenotypes associated with *invadolysin* mutants were increased levels of nuclear envelope proteins and defective germ cell migration in embryos (McHugh et al., 2004).

We observed intriguing localization patterns in cultured human cells with antibodies generated against recombinantly expressed human invadolysin. The protein localized to 'ring-like' structures postulated to be invadopodia in cultured cells and to the leading edge of migrating macrophages. This suggested that invadolysin may participate in cell migration, which we subsequently demonstrated by examining germ cell migration in *Drosophila* embryos (McHugh et al., 2004). We report here the existence of four *invadolysin* splice variants, compare their conservation within the M8 family of metalloproteases and show that invadolysin is associated with cytoplasmic lipid droplets, both by immunofluorescence and subcellular fractionation. Thus, invadolysin is the first identified metalloprotease located on these dynamic organelles and we discuss its functional significance.

Results

Invadolysin gene structure and relationship to other M8 metalloproteases

The M8 metalloproteases (whose active site consensus sequence is HEIXHALGFS) include not only invadolysin but also members varying in size from 283 amino acids in *Bradyrhizobium japonicum* (accession: NP_772671) to 1267 amino acids in *Dictyostelium discoideum* (accession: EAL67289) and several leishmanolysin-like (LMLN) paralogues in various kinetoplastids (Fig. 1A). For example, *Leishmania major* has six known distinct LMLN proteins (Ivens et al., 2005) and *Leishmania braziliensis* has at least 32 distinct LMLN proteins, whereas the *Trypanosoma cruzi* genome appears to encode well over a hundred distinct LMLN proteins.

Leishmanolysin itself is a major glycosylphosphatidylinositol (GPI)-linked surface protease found in high abundance on the surface of promastigotes (Etges, 1992; Yao et al., 2003). By contrast, GPI-anchored proteins are generally less abundant in higher eukaryotes (McConville and Ferguson, 1993) and most animal and plant species for which sufficient genomic sequence is available

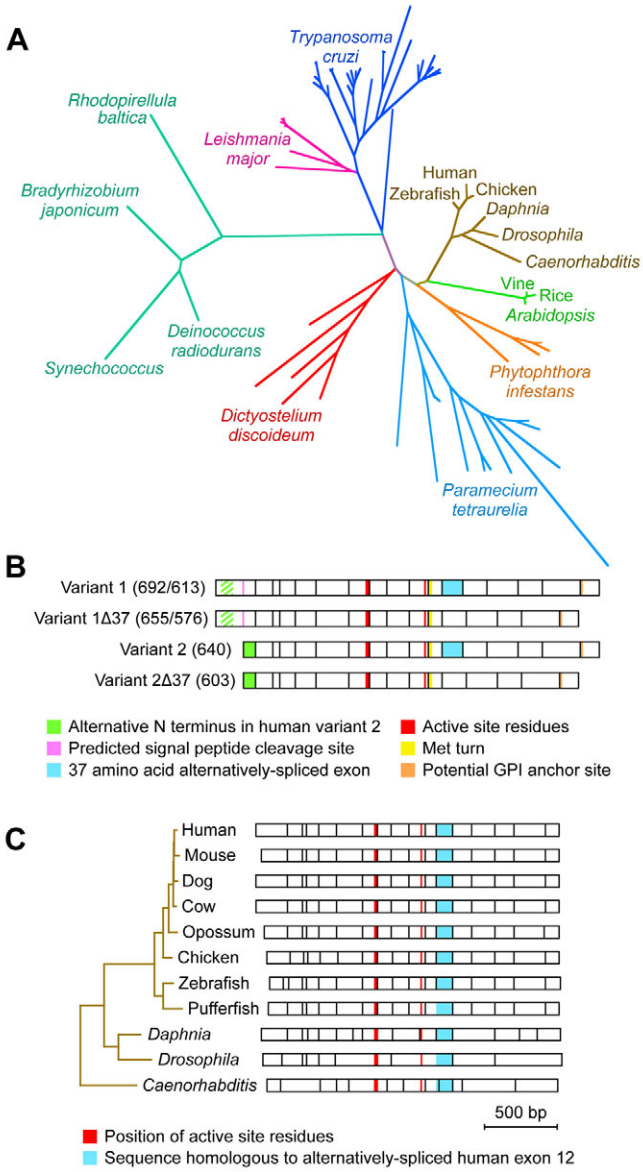

Fig. 1. Phylogenetic analysis and identification of different invadolysin splice variants. (A) Phylogenetic tree showing the relationship of the invadolysin protein found in animals to other representatives of the M8 family of metalloproteases in plants, selected protozoa and bacteria. (B) Four splice variants of invadolysin identified in human cells, showing the location of variant exons and motifs predicted to be functionally significant. The location of the alternative first exon of variant 2 nested within that of variant 1 is indicated by green cross-hatching. The sizes (in amino acids) reflect predicted processing of signal sequences and addition of GPI anchors to variant 1 forms. (C) Schematic diagram depicting exon boundaries of the invadolysin gene in different animals, together with a phylogram representing the evolutionary relationship between corresponding protein sequences. Sequences are aligned based on the location of conserved catalytic histidine residues (shown in red) and the 37 amino acid region corresponding to that encoded by exon 12 of the human invadolysin gene is shaded blue. Bootstrap scores for trees and details of aligned sequences are available in supplementary material Table S1.

seem to have only one *LMLN* gene. Although no M8 metalloproteases were found in any yeast species or other true fungi, the genome of *Phytophthora infestans* (which belongs to the oömycetes or 'water moulds') contains four *LMLN* genes and the slime mould *Dictyostelium discoideum* has five such genes. Several *LMLN* genes are also apparent in ciliates such as *Paramecium tetraurelia* and at least two such genes are found in representatives of the *Entamoeba* genus. Interestingly, M8 metalloprotease genes are found not only in eukaryotes but also in several bacterial species (Fig. 1A). However, no such genes are apparent in any archaeal genomes sequenced to date and they have also not yet been found in *Guillardia theta*, *Giardia lamblia* or members of the apicomplexa. Therefore, M8 metalloproteases are found in a diverse array of organisms, in which the number of gene copies can vary enormously.

Although only one *LMLN* gene has been found in most animals (among which it is known as *invadolysin*), we have identified four distinct splice variants in human cells (Fig. 1B). Variants for which the N-terminus is encoded by the longer first exon of variant 1 (accession: AM920777 or AJ312399) are predicted to encode a signal peptide, in addition to a predicted C-terminal site for GPI modification. Additional human splice variants have been identified in which the N-terminus is encoded by an alternative variant 2 first exon (the sequence of which is nested within the variant 1 first exon but translated in a different reading frame). Such variant 2 transcripts (accession: AJ312398 or AM920778) lack the predicted signal peptide cleavage site and may therefore have a different intracellular localization (although they still encode the C-terminal site for potential GPI modification). Each of these human *invadolysin* N-terminal splice variants may also exist in two alternative forms differing by the presence (accession: AM920777 or AJ312398) or absence (Δ37 form, accession: AJ312399 or AM920778) of a 37 amino acid region encoded by exon 12. If translated, the structure of Δ37 variant proteins is expected to differ markedly from +37 variants, judging by the location of a homologous sequence spanning ~44 Å in the structure of leishmanolysin (Schlagenhauf et al., 1998).

This alternatively spliced 37 amino acid sequence is encoded by a distinct exon in *invadolysin* genes from tetrapod vertebrates (Fig. 1C) and zebrafish (*Danio rerio*) but not in the pufferfish *Tetraodon nigroviridis* or available genomes of other teleosts. Although the homologous sequence is represented by a distinct exon in the crustacean *Daphnia pulex*, it is fused to the previous exon in *Drosophila* and various other insects, whilst most of the corresponding region is encoded by a single distinct exon in the nematode *Caenorhabditis elegans*. Therefore, the alternatively spliced exon 12 of humans is conserved as a distinct exon in diverse lineages. By contrast, the alternative first exon utilised in human variant 2 does not appear to have a counterpart in the available sequences of other species (aside from orang-utan or chimpanzee) because of the absence of a start codon similarly nested in a different reading frame.

Four *invadolysin* splice variants are expressed in human cells

The existence of four variants in different human cells was verified by RT-PCR with primers designed to selectively amplify specific variants, as depicted in Fig. 2A,C, and confirmed by sequencing. Examples of such reactions are shown in Fig. 2B, in which the shorter bands corresponding to the variant 2 products appear significantly less abundant than the variant 1 products. Reactions performed with primer combinations designed to amplify larger products specific to particular variants (supplementary material Fig. S1) also suggest a greater abundance of variant 1. Similar time courses of RT-PCR were performed to estimate the relative abundance of +37 and Δ37 variants (Fig. 2D). In all cases, the +37 variants appeared roughly twofold more abundant than Δ37 variants. The relative abundance of different human *invadolysin* variants

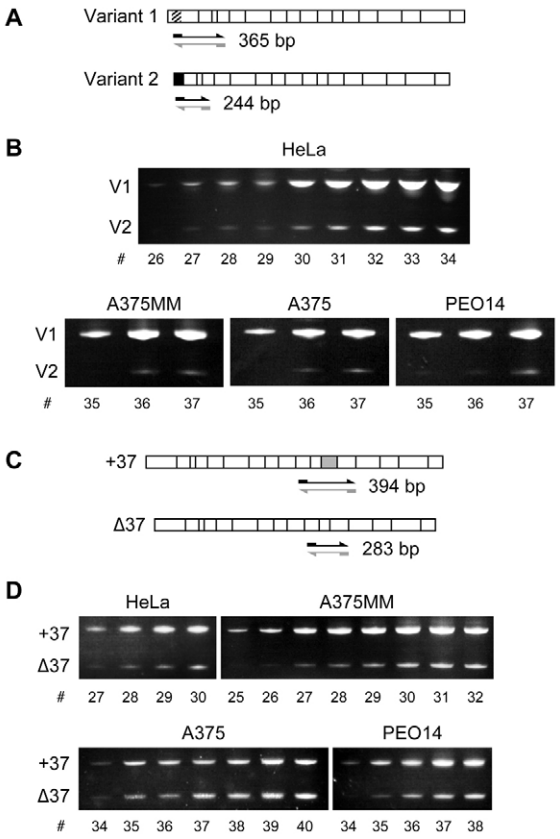

Fig. 2. Determination of the relative abundance of different human invadolysin splice variants. (A) Map showing the relative location of the Hv2f and Hv2r primer combination and the expected size of PCR products amplified from different N-terminal variants. (B) Time course of RT-PCR reactions using the Hv2f and Hv2r primer combination after the indicated number of cycles (#) in HeLa, A375MM, A375 and PEO14 cells. Variant 1 (V1) is considerably more abundant than variant 2 (V2) based on the relative intensity of the respective 365 bp and 244 bp bands after different cycles of amplification. (C) Map showing the relative location of the H12f and H12r primers flanking exon 12 and the expected size of PCR products amplified from different variants. (D) Time course of RT-PCR reactions using the H12f and H12r primers. The upper 394 bp product band corresponding to variants containing the 37 amino acid region encoded by exon 12 generally appears more abundant than the 283 bp band corresponding to Δ37 variants.

could thus be estimated, suggesting that v1+37 is the most prevalent, whereas v2Δ37 may be the least abundant of all currently known variants.

Alternative splicing events might also occur in other metazoan species to yield +37 and Δ37 invadolysin variants. PCR reactions performed in mouse, rat, cow, chicken, zebrafish and *Daphnia* tissue extracts only amplified a product of the expected size for +37 variants but no smaller product representing a Δ37 variant was observed (supplementary material Fig. S2; and data not shown). However, both +37 and Δ37 variants were readily detectible in orang-utan and rhesus macaque by RT-PCR (supplementary material Fig. S3). PCR reactions performed on cDNA from mouse and macaque with primers for the N-terminal region were only able to amplify a product corresponding to variant 1, with no smaller bands corresponding to variant 2 transcripts (supplementary material Figs S2 and S3). The inability to detect a variant 2 transcript in mouse and macaque is consistent with the absence of an alternative start codon nested within a different reading frame of the first exon. Nevertheless, PCR reactions performed on orang-utan cDNA indicate that the same variants found in humans are conserved in other hominids.

Invadolysin is present in all cell lines analyzed

Polyclonal antibodies were generated against different regions of human invadolysin (Fig. 3A), one recognizing the peptide YRGGKWPHGAVGVP (P1-Ab), one recognizing the peptide CDFVRKSCKFWIDQQ (P2-Ab), and two antibodies (C-Ab1 and C-Ab2) raised against a C-terminal his-tagged fusion protein (residues 327-629 of v1Δ37). We previously reported immunofluorescence results using C-Ab2 (McHugh et al., 2004), which labelled ring-like structures of ~1 μm in diameter in HeLa cells. Although affinity-purified C-Ab2 antibody also labelled 'rings' in cells, more than one band was recognized on immunoblots of whole cell lysates. P1-Ab, C-Ab1 and C-Ab2 were therefore immunoblotted against GST-fusion-protein constructs containing nearly full-length invadolysin sequences, to confirm antigen recognition (Fig. 3B). Each antibody recognized both the +37 and Δ37 GST-fusion protein constructs. The antibodies were next used to probe A375MM whole cell lysates. The antibodies all recognized a band of 83 kDa (Fig. 3C), which is similar to the predicted molecular mass of 78 kDa for the full-length (unprocessed) v1+37 variant (proposed to be most abundant). A band of the same size was also detected using C-Ab1 against lysates from several different cell lines, appearing especially abundant in HBL human melanoma cells compared to the α-tubulin loading control (Fig. 3D).

Annular structures of similar size and shape were also found in each cell type probed by immunoblotting, though some cell lines contained different numbers of these rings (Fig. 4). As several well-defined ring-like structures were consistently observed in A375 and A375MM human melanoma cells, these were selected for further study.

Invadolysin and invadopodia

Previously, co-staining of C-Ab2 with different markers for subcellular compartments (Golgi, mitochondria, lysosomes and components of the proteasome or signalosome) failed to unambiguously identify what the rings were (McHugh et al., 2004). Based on its localization to the leading edge of migrating human macrophages and its importance for migration of *Drosophila* germ cells, we proposed that invadolysin may participate in cell movement and invasion via invadopodia, which exhibit a similar ring-like appearance by conventional fluorescence microscopy (Baldassarre et al., 2003).

Invadopodia are found at the leading edge of migrating cells or near the basal surface of cultured cells (Ayala et al., 2006; Marx, 2006), characterized by colocalization of actin-rich puncta with foci of extracellular matrix degradation (Baldassarre et al., 2006; Linder and Kopp, 2005). We therefore examined the localization of invadolysin rings relative to substrate degradation by invadopodia. Although immunostaining for cortactin was enriched at sites of FITC-gelatine degradation (supplementary material Fig. S4), invadolysin did not colocalize with invadopodial structures defined by cortactin and FITC-gelatine degradation.

Invadolysin localizes on the surface of lipid droplets

In the absence of significant colocalization between invadolysin and various subcellular markers or invadopodia, we postulated that the circular structures might represent endocytic vesicles. We therefore utilized functional assays for clathrin-mediated and caveolar endocytosis. Fluorescently labelled transferrin added to

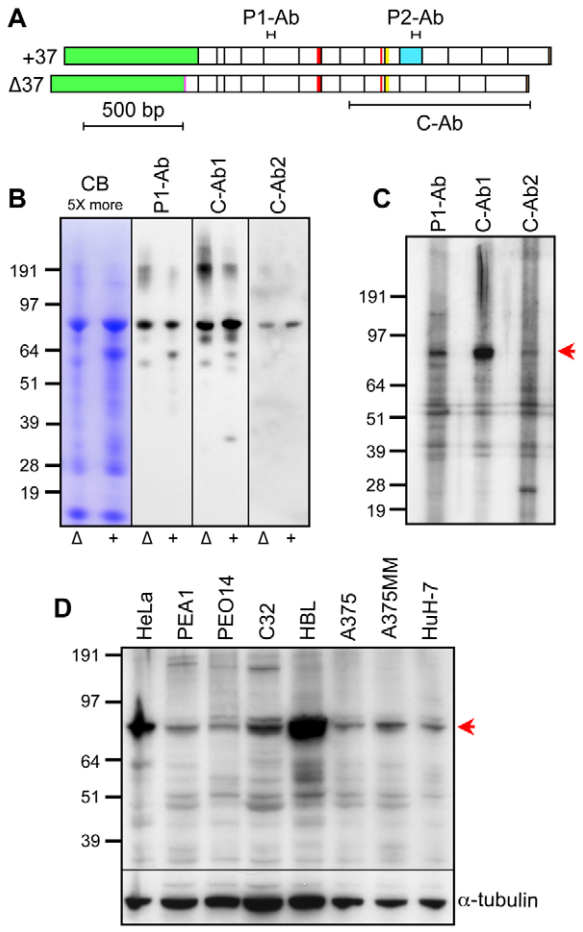

Fig. 3. Characterization of invadolysin antibodies. (A) GST fusion constructs (green) close to the N-terminus of invadolysin (+37 and Δ37 variants) were generated. These constructs contained the antigenic regions used to generate the invadolysin antibodies (as indicated by P1-Ab, P2-Ab and C-Ab). (B) Bacterially expressed and purified GST constructs were resolved and visualized with Coomassie blue staining (CB, left panel) or immunoblotted with P1-Ab, C-Ab1 or C-Ab2. The Coomassie-stained lanes contained fivefold more protein than the immunoblotted lanes. (C) Whole cell lysate of A375MM melanoma cells was loaded into a 1-well gel, and immunoblotted with P1-Ab, C-Ab1 or C-Ab2. All antibodies recognized a band of the same size (red arrow). (D) C-Ab1 recognizes invadolysin (red arrow) in whole cell lysates from several different cell lines (indicated above the gel).

culture medium is routinely used as a marker for clathrin-mediated endocytosis (Rappoport and Simon, 2003). When cells were incubated with Cy5-labelled transferrin, the internalized transferrin was not detected inside invadolysin rings, suggesting the rings were not directly associated with clathrin-mediated endocytosis (data not shown). Further immunofluorescence experiments using clathrin or dynamin 1 antibodies revealed a similar lack of colocalization with invadolysin, consistent with the transferrin uptake results (supplementary material Fig. S5).

To examine caveolar endocytosis, fluorescently labelled cholera toxin B (CtxB) was used as a tracer (Orlandi and Fishman, 1998). When cells were treated with CtxB for 10 minutes and stained with antibodies for invadolysin, the toxin could easily be detected inside invadolysin rings (supplementary material Fig. S6A), suggesting that invadolysin rings might be associated with caveolae. CtxB could also be detected in other parts of the cell following incubation for 20 minutes but the localization within invadolysin rings was more apparent when cells were treated for a shorter time period. This suggested that CtxB associated transiently with invadolysin rings, which themselves might be a lipid-based entity as CtxB has an affinity for GM_1 glycosphingolipids. However, only a partial colocalization was initially observed between caveolin 1, a caveolar marker protein (Rothberg et al., 1992), and invadolysin (data not shown). Therefore, cells were treated with brefeldin A, which blocks vesicle trafficking from the endoplasmic reticulum to the Golgi apparatus and increases the localization of caveolin to the lipid droplets (Fujimoto et al., 2001; Ostermeyer et al., 2001; Pol et al., 2004). Following treatment with brefeldin A, invadolysin colocalized with caveolin and appeared to surround vesicles to generate ring-like structures (supplementary material Fig. S6B).

Intriguingly, caveolin 1 and caveolin 2 are recruited to lipid droplets and appear as ring-like structures upon oleic acid treatment of cultured cells (Pol et al., 2004). Lipid droplets are typically large (~1-20 μm in diameter) and almost spherical, so proteins localized to the surface would have a characteristic ring-like appearance by conventional fluorescence microscopy (Thiele and Spandl, 2008; Welte, 2007). Oleic acid accumulates in lipid droplets, which grow in size in response to this fatty acid (Brasaemle et al., 1997). To examine whether the invadolysin rings encircled a lipid-based entity, we treated cells with increasing concentrations of oleic acid. Indeed, the diameter of invadolysin rings increased markedly following oleic acid treatment, suggesting that invadolysin rings might surround lipid droplets (Fig. 5).

Several protein components of lipid droplets, such as PAT family proteins (perilipin, ADRP, TIP47), have a ring-like appearance surrounding the core of neutral lipids (Wolins et al., 2006). Immunofluorescence detection of TIP47 (tail interacting protein of 47 kDa) or ADRP (adipose differentiation related protein) revealed rings similar to those observed after labelling for invadolysin (Fig. 6A; and data not shown). The size and morphology of the TIP47 and ADRP rings, bona fide components of the surface of cytoplasmic lipid droplets, were comparable to invadolysin rings. Lipid droplets labelled with BODIPY were clearly surrounded by TIP47 protein. When cells were similarly co-stained with invadolysin and BODIPY, strikingly, a core of lipid droplet staining was detected inside every invadolysin ring (Fig. 6B). The localization of invadolysin with BODIPY was also examined in HuH-7 human hepatocarcinoma cells, which are known to contain numerous lipid droplets (Targett-Adams et al., 2003), and invadolysin was similarly detected at the surface of these structures (Fig. 6C).

To independently confirm that invadolysin was associated with lipid droplets, we isolated lipid droplets from cultured cells. We immunoblotted subcellular fractions with different invadolysin antibodies and observed a striking enrichment of invadolysin in the lipid droplet fraction (Fig. 7). This enrichment was observed with three different antibodies recognizing distinct epitopes of invadolysin (but not with a commercial antibody generated to what is reported to be within the processed prodomain of invadolysin). In conclusion, the presence of invadolysin on the surface of lipid droplets provides the first demonstration of a metalloprotease localizing to this intriguing and dynamic organelle. Absence of signal with an antibody generated to the putative prodomain of invadolysin further suggests the form on lipid droplets may be processed, and potentially active.

In light of our evidence that invadolysin associates with lipid droplets, we then investigated whether loss of invadolysin function affects lipid storage in *Drosophila*. The fat body of *Drosophila* is

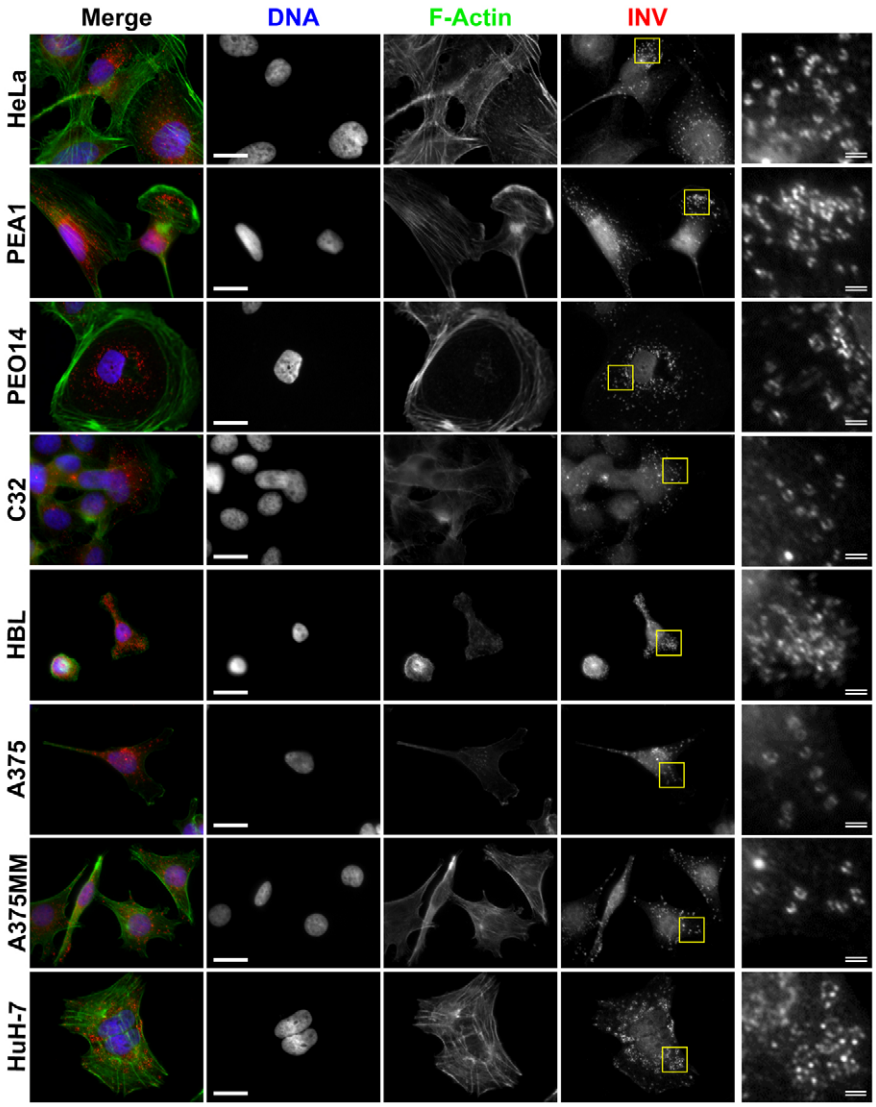

Fig. 4. Invadolysin antibodies visualize a ring-like structure in different cultured cells. Different cell lines were stained for DNA with DAPI (blue), F-actin with phalloidin (green) and invadolysin (red). Boxed areas are enlarged in the far right panel. Scale bars: 20 µm in the DNA images; 2 µm (double white lines) in the far right panels.

a sheet-like structure composed of adipocytes that stores lipids and supplies the animal with energy throughout development (Grönke et al., 2003; Schlegel and Stainier, 2007). We, therefore, examined the fat body of larvae homozygous for the *IX-14*^{4Y7} allele, in which *invadolysin* is undetectable by northern blotting (McHugh et al., 2004). As shown in Fig. 8A-D, when larval fat bodies were stained with Nile Red to visualise lipid droplets, it became apparent that the thickness of the fat body and the cross sectional area of constituent cells were significantly reduced in *IX-14*^{4Y7} mutant larvae (Fig. 8E). To more directly examine the effect of loss of invadolysin function on lipid storage, we measured the level of stored triglyceride relative to total protein content in whole larvae. The ratio of triglyceride to protein was significantly reduced in *IX-14*^{4Y7} mutant larvae compared with wild-type larvae (Fig. 8F), which is a similar effect to that observed in *Lsd2*^{KG00149} (a PAT family protein) mutants, in which the fat body is less developed (Grönke et al., 2003; Teixeira et al., 2003).

Discussion

Our phylogenetic analyses have revealed that homologues of invadolysin are conserved in many different organisms, in which the gene copy number can vary considerably. It is possible that the multiple copies of LMLN proteins in the trypanosomatids may reflect domination of their cell surface by GPI-anchored proteins that form a protective coat and facilitate evasion of the host immune system (Ilgoutz and McConville, 2001).

Bearing in mind the previous characterization of invadolysin as a protein associated with cell migration in animals (McHugh et al., 2004), the lack of any M8 metalloproteases in the available genomes of yeast species might reflect the absence of cell migration in fungi such as yeasts. Given the lack of M8 metalloproteases in a choanoflagellate (King et al., 2008) and a placozoan (Srivastava et al., 2008), secondary loss of such genes may be a more general feature of simpler opisthokonts. By contrast, five *LMLN* genes are found in the slime mould *D. discoideum*, in which invasive cell migration is known to occur during amoeboid motion (Fukui et al., 1999). Moreover, multiple *LMLN* genes are apparent in the genome of the water mould *P. infestans*. As *P. infestans* is a haustoria-producing pathogen that parasitizes members of the Solanaceae, perhaps surface expression of a GPI-anchored protease may play a role in host-pathogen interactions (Birch et al., 2006). Although invasive cell migration also notably occurs during pollen tube

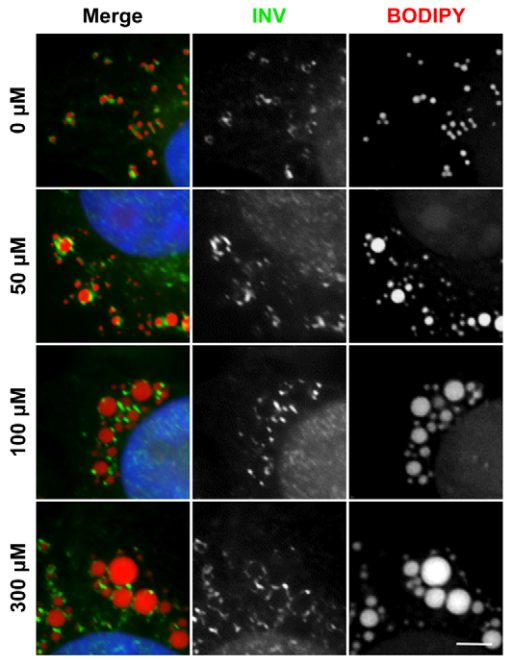

Fig. 5. Oleic acid treatment increases the size of invadolysin rings. A375 cells were treated with oleic acid (50, 100 or 300 µM) for 24 hours and stained for invadolysin (green), for lipid droplets with the neutral lipid dye BODIPY 630/650 (red) and for DNA with DAPI (blue in merged image). The diameter of the invadolysin rings surrounding lipid droplets increased proportionately with increasing oleic acid concentrations. Scale bar: 2 µm.

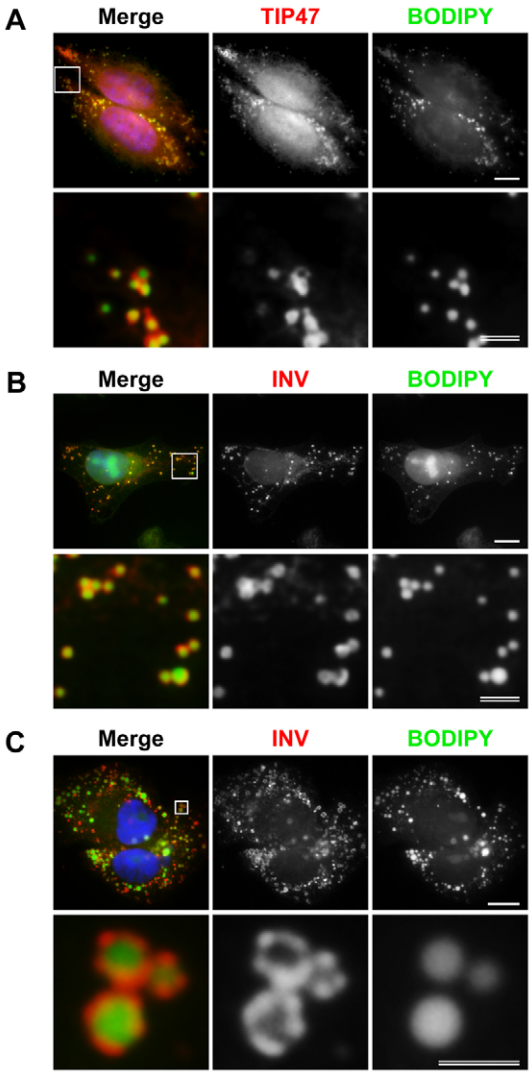

Fig. 6. Invadolysin localizes to lipid droplets. (A) A375 cells stained for TIP47 (red), lipid droplets with neutral lipid dye BODIPY 493/503 (green), and DNA with DAPI (blue in merged image). Boxed areas are enlarged below. (B) A375 cells stained for invadolysin (red), for lipids with BODIPY 493/503 (green), and DNA with DAPI (blue in merged image). Both TIP47 and invadolysin surround BODIPY-labelled lipid droplets. (C) HuH-7 cells were stained for invadolysin (red), for lipids with BODIPY 493/503 (green), and DNA with DAPI (blue in merged image). BODIPY staining was always surrounded by invadolysin rings indicating that invadolysin is localized on the surface of lipid droplets. Single scale bars: 10 µm; double scale bars: 2 µm.

growth (Gossot and Geitmann, 2007), the potential role of M8 metalloproteases in plants remains enigmatic, as cell wall loosening in grasses does not appear to require proteolytic activity (Li and Cosgrove, 2001), but another zinc metalloprotease is reported to mediate cell wall digestion prior to gamete fusion in *Chlamydomonas* (Kinoshita et al., 1992). Therefore, the conservation of M8 metalloproteases arguably could be partly related to more invasive eukaryotic cell migration, although conservation of bacterial homologues may reflect more ancient activities.

The human *invadolysin* gene encodes four distinct splice variants, differing by the presence or absence of an N-terminal signal peptide and/or an exon encoding 37 amino acids. Comparing the sequences of invadolysin in other species indicates that the signal peptide is a conserved feature, despite more general N-terminal sequence divergence. Given that signal peptides play a central role in the targeting and translocation of nearly all secreted proteins and many integral membrane proteins (Zheng and Gierasch, 1996), we anticipate that the more conserved (and prevalent) splice variants of human invadolysin, containing such sequences, would be membrane localized. The 37 amino acid sequence encoded by exon 12 of human invadolysin is conserved not only between metazoan orthologues but also amongst more divergent M8 metalloproteases. As a homologous sequence spans the N- and C-terminal regions of leishmanolysin (Schlagenhauf et al., 1998), we anticipate that any Δ37 invadolysin proteins should differ considerably in structure and expected activity and may even function to regulate invadolysin's activity.

However, it is presently unclear whether distinct roles might be played by the four splice variants identified in hominids, especially given that not all have been identified in most other species examined. Although a rarer Δ37 variant was detected in rhesus macaque, no variant 2 transcript was found. As human variant 1 invadolysin is far more prevalent than variant 2, and human +37 transcripts are more abundant than Δ37 transcripts, the most abundant human invadolysin splice variant is also the one most conserved amongst related species.

Invadolysin appears to be ubiquitously expressed, as the protein is present in all cell lines tested and has also been detected in a wide range of mouse organ extracts by immunoblotting (supplementary material Fig. S2). Although invadolysin was previously demonstrated to be essential for germ cell migration in *Drosophila* embryos and the human protein was observed at the

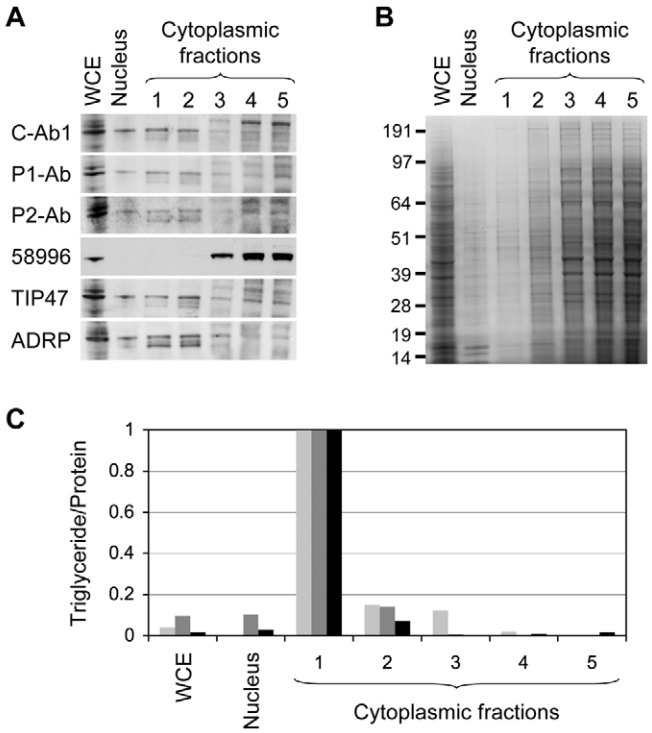

Fig. 7. Invadolysin is enriched in isolated lipid droplets. (A) Immunoblot of A375 cell fractions with different antisera detecting invadolysin (C-Ab1, P1-Ab, P2-Ab, and 58996 – a commercial antibody to the putative prodomain), TIP47 and ADRP. Equal volumes of each fraction were loaded in separate lanes. The uppermost fraction containing lipid droplets is numbered 1, with the lowermost cytoplasmic fraction numbered 5. (B) A375 cell fractions visualized with Coomassie Blue staining, demonstrating different protein concentrations in the obtained fractions. (C) Normalised ratios of triglyceride to protein in different fractions of A375 cells from three separate subcellular fractionation experiments (indicated by different shades of grey). WCE, whole cell extract.

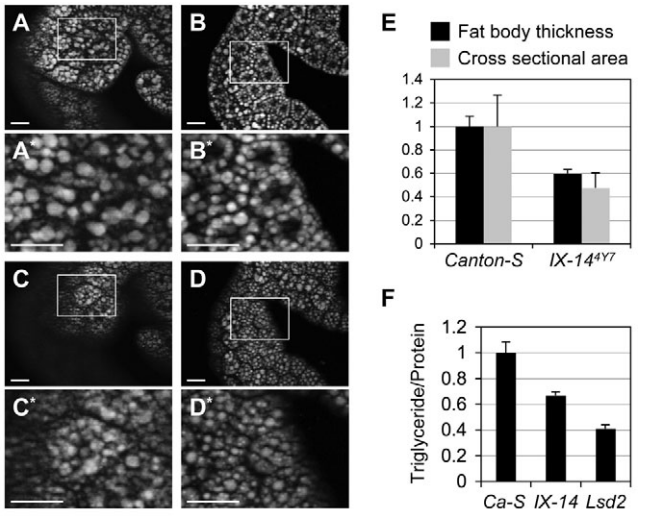

Fig. 8. Loss of invadolysin function affects development of the fat body in *Drosophila*. Visualisation of lipid droplets within cells of the fat body from Canton-S (A,C) and *IX-14*^{4Y7} (B,D) third instar larvae. (A*,B*,C*,D*) Enlarged images of the boxed areas in the A-D, respectively. Scale bars: 50 μm. (E) Normalised mean thickness of fat body and cross sectional area of cells containing lipid droplets, with standard deviations. (F) Normalised ratios of triglyceride content relative to total protein content in whole third instar wild-type and mutant larvae, with associated standard deviation.

leading edge of migrating macrophages (McHugh et al., 2004), invadolysin does not appear to coincide with structures identified as invadopodia. Instead, we have shown that the ring-like subcellular localization of invadolysin surrounds lipid droplets, and that invadolysin can be found on the surface of lipid droplets in several cell lines.

We have been able to demonstrate by immunofluorescence detection that invadolysin is present on intracellular lipid droplets and have also detected it on lipid droplets isolated by fractionation of cultured cells. Three different antibodies to invadolysin, generated against distinct epitopes of the protein, all recognize a band of 53 kDa by immunoblotting the lipid-droplet-containing top fractions, collected after floatation on sucrose gradients. It is therefore tempting to speculate that this band represents a form processed from a precursor full-length protein. Whether this form is proteolytically active is currently being investigated.

Lipid droplets (or 'lipid bodies') are dynamic organelles associated with several diverse processes in addition to the storage of neutral lipids (Welte, 2007). They have been implicated not only in lipid turnover (Smirnova et al., 2006) and cholesterol homeostasis (Naslavsky et al., 2007) but also in cancer (Accioly et al., 2008), hepatitis C infection (Miyanari et al., 2007) and Parkinson's disease (Scherzer and Feany, 2004). Lipid droplets also function in both proteasomal and lysosomal degradation of apolipoprotein B (Ohsaki et al., 2006) and as transient storage depots for proteins, such as core histones in *Drosophila* embryos (Cermelli et al., 2006). Although it is possible that invadolysin may be similarly sequestered on lipid droplets for later use, it could conceivably be proteolytically active. If so, it may be of particular relevance that invadolysin was previously implicated in lamin cleavage (McHugh et al., 2004), given that lamin was found in lipid droplets from *Drosophila* embryos (Cermelli et al., 2006).

In an attempt to address whether the presence of invadolysin on lipid droplets may be of functional significance, we have begun to characterize the appearance of lipid droplets and the triglyericide to protein ratio in the *invadolysin* mutant. As shown in Fig, 8, the fat body and its constituent cells are smaller in the *invadolysin* mutant, and the triglyceride to protein ratio approaches that observed for the *Lsd2* mutation in *Drosophila*. Thus, these results point towards a role for invadolysin – either directly or indirectly – in lipid droplet dynamics in *Drosophila*.

It has recently been shown that GPI-anchored proteins can be transiently associated with lipid droplets (Müller et al., 2008). Since v1+37 and v1Δ37 invadolysin variants are predicted to contain a GPI anchor, it is plausible that these variants may be additional examples of lipid droplet-associated GPI-anchored proteins. Given that invadolysin localizes to the leading edge of migrating macrophages (McHugh et al., 2004), it is noteworthy that increased numbers of lipid droplets in leukocytes are often associated with infectious and inflammatory conditions (D'Avila et al., 2008). Stimulation of phagocytosis in macrophages has also been described as leading to accumulation of lipid droplets around phagosomes (van Manen et al., 2005). However, details of the triggering process and molecular mechanisms involved in lipid droplet formation remain a focus of some debate in the absence of a correlation with bacterial phagocytosis (D'Avila et al., 2008). Instead, it appears that the increase in lipid droplet number during infection may be largely

related to synthesis of eicosanoids such as prostaglandin-E2 (D'Avila et al., 2008), which may otherwise inhibit macrophage phagocytosis (Aronoff et al., 2004) and bactericidal capacity (Serezani et al., 2007). Whether invadolysin plays a particular role in modulating such macrophage activities is the subject of ongoing research.

Meanwhile, the existence of possible connections between lipid droplet formation and cell migration have yet to be fully explored. At least one lipid droplet protein (ADRP) is transcriptionally activated relatively early in the development of renal cell carcinoma, though its expression is gradually downregulated during subsequent stages of tumorigenesis and metastasis (Yao et al., 2007). Since increased numbers of lipid droplets have been observed in neoplastic colon cancer cells (Accioly et al., 2008), the role of these organelles in transformation and spread of cancer cells warrants further study. As inhibition of intracellular membrane trafficking blocked extracellular matrix degradation by invadopodia (Ayala et al., 2006) and endocytosis has been linked with cell migration (Grande-Garcia and del Pozo, 2008; Rappoport and Simon, 2003), it remains possible that lipid droplet-associated invadolysin might influence cell migration via invadopodia, albeit less directly than we previously suspected.

As with other proteins seemingly sequestered in lipid droplets (Welte, 2007), several questions remain regarding the status of invadolysin associated with these organelles. It will be important to ascertain whether the protein is catalytically active and what proteins invadolysin may interact with on lipid droplets. In light of similarities between eukaryotic lipid droplets and neutral lipid bodies in bacteria (Waltermann and Steinbuchel, 2005), it is tempting to speculate that bacterial M8 metalloproteases might similarly associate with such organelles. However, the phylogenetic distribution of M8 metalloproteases does not correspond to that of conserved proteins reportedly inducing lipid droplet accumulation (Kadereit et al., 2008), or the ability of oleogenic fungi lacking obvious invadolysin homologues to accumulate high levels of lipid bodies (Murphy, 2001). By contrast, various separate groups of structural proteins associated with lipid droplets (PAT family proteins in animals and *Dictyostelium*, caleosins in plants and fungi, oleosin from plants and bacterial phasins) share no obvious homology with each other and are thought to have arisen independently. Therefore, it is possible that recruitment of invadolysin to lipid droplets may be restricted to a subset of species.

In conclusion, the identification of invadolysin as the first metalloprotease localizing to the surface of lipid droplets raises a host of questions deserving further investigation. Current studies are focused on extending analyses of lipid droplet dynamics and homeostasis in *Drosophila* mutants. Determining the activity of invadolysin in association with lipid droplets should yield valuable new insights about a hitherto poorly understood organelle that is nevertheless of great importance to normal and disease states.

Materials and Methods

Phylogenetic analysis

The region of the invadolysin protein used for phylogenetic reconstruction of M8 metalloproteases from a range of species was initially derived by aligning each protein sequence, extracted from public databases, with that corresponding to the crystal structure for gp63 (PDB code: 1LML), using the HHpred interactive server (Soding et al., 2005). The resulting protein sequences were then aligned in smaller groups using the T-Coffee program (Notredame et al., 2000) and these were combined into larger multiple sequence alignments by performing profile alignments with ClustalW (Thompson et al., 1994) followed by manual adjustment. In the case of invadolysin sequences from representative animal species, the whole protein sequence was aligned rather than the aforementioned central region. Phylogenetic trees were calculated using TREE-PUZZLE (Schmidt et al., 2002) and the Proml program of the PHYLIP Package (http://evolution.genetics.washington.edu/phylip.html), generating smaller trees separately of more closely related sequences and then combining these in larger assemblages (selecting optimal tree topologies using the combined criteria of maximum likelihood and minimum evolution along all branch lengths). The branch lengths of trees presented here were calculated using the Whelan-Goldman model of amino acid substitution (Whelan and Goldman, 2001), with rate heterogeneity among sites modelled according to a gamma distribution with 16 rate categories. The gamma distribution shape parameter was estimated from the data set using TREE-PUZZLE and bootstrap scores of trees in the supplementary material were obtained from 1,000 replicates using the Seqboot and Consense programs of the PHYLIP Package (http://evolution.genetics.washington.edu/phylip.html).

Chemicals and reagents

All chemicals were obtained from Sigma-Aldrich unless otherwise noted. PEA1 and PEO14 (human ovarian carcinoma) cell lines were kindly provided by Grant Sellar (Wyeth Research, Dundee, UK). A375, C32 and HBL (human melanoma) cell lines were generously provided by David Melton (University of Edinburgh, UK). A375MM (an invasive subclone of A375) was kindly provided by Laura Machesky (Beatson Institute, Glasgow, UK), the HeLa cell line (epithelial cervical carcinoma) was generously donated by William Earnshaw (University of Edinburgh) and Huh7 human hepatocarcinoma cells were kindly provided by Jim Ross (University of Edinburgh). Cells were maintained at 37°C, 5% CO_2 in DMEM (Invitrogen) supplemented with 10% FBS (Sigma). Percoll-fractionated primary monocytes were kindly supplied by Adriano Rossi (University of Edinburgh) and directly used for RNA experiments. A Sumatran orang-utan (*Pongo pygmaeus abelii*) B-cell line (PPY00327IN) was provided by Gaby Doxiadis at the Biomedical Primate Research Centre (BPRC) in the Netherlands, from which RNA was extracted following culture of cells in RPMI 1640 (+ L-glutamine; Invitrogen) supplemented with 10% FBS (Sigma).

RT-PCR

RNA was extracted using the RNeasy mini kit (Qiagen) from tissues previously immersed in RNAlater (Qiagen) or from cultured cells following treatment with TRIzol Reagent (Invitrogen). Reverse transcription reactions using an oligo(dT) primer were performed with AffinityScript Multiple Temperature cDNA synthesis kit (Stratagene), according to the manufacturer's instructions. In addition, cDNAs for human, mouse and rhesus macaque were obtained from CytoMol Unimed (Sunnyvale, CA). PCR reactions were performed with Herculase Hotstart DNA Polymerase (Stratagene), according to the manufacturer's instructions. PCR reactions were performed using an annealing temperature of 57°C with primers designed to span exon boundaries (supplementary material Table S2).

Antibody production

Peptides were synthesized after determination of the peptide sequences. Rabbit polyclonal antibodies (P1-Ab and P2-Ab) was generated by Genosphere Biotechnologies (Paris, France) and rabbit polyclonal antibodies (C-Ab1 and C-Ab2) were generated in conjunction with Diagnostics Scotland (Penicuik, Scotland, UK).

Purification of GST-recombinant proteins

Fragments encoding different portions of invadolysin were generated by PCR of cDNAs and fused in-frame to glutathione *S*-transferase (GST) in the pGEX-4T plasmid (Amersham, Piscataway, NJ). Overexpression and affinity purification of GST-recombinant proteins was based on previously described work (Frangioni and Neel, 1993). In brief, an overnight culture (1 ml) was added to 100 ml fresh Luria Bertani (LB) medium containing 100 μg/ml ampicillin and grown to an OD_{600} of 0.6. Expression was induced with 0.4 mM isopropyl β-D-1-thiogalactopyranoside (IPTG) for 3-4 hours at 30°C. After induction, bacterial cells were pelleted and washed with ice-cold STE buffer (10 mM Tris, pH 8.0, 150 mM NaCl, 1 mM EDTA). The pellet was then suspended in 6 ml STE buffer containing 100 μg/ml lysozyme and protease inhibitors and incubated on ice for 15 minutes. Bacteria were lysed by adding sarkosyl to STE buffer (0.5% final concentration) and sonicating the lysate. Extracts were clarified by centrifugation. Supernatants were adjusted to contain 2% Triton X-100 and incubated with glutathione beads for 2 hours. The beads were washed six times with ice-cold wash buffer (10 mM Tris, pH 8.0, 200 mM NaCl, 1 mM EDTA) and resuspended in storage buffer (50 mM Hepes, pH 7.5, 150 mM NaCl, 1 mM DTT, 10% glycerol). GST-fusion protein was eluted from glutathione beads by boiling in SDS-PAGE sample buffer (2% SDS, 50 mM Tris pH 6.8, 10% glycerol, 0.01% Bromophenol blue, 2 mM EDTA, 20 mM DTT).

Immunoblotting

Protein extracts or GST constructs were electrophoresed on either 1- or 15-well 4-12% NuPAGE BT SDS-PAGE gels (Invitrogen) in MOPS buffer and transferred to nitrocellulose membranes as described previously (McHugh et al., 2004). Membranes were washed twice with TBSTw (TBS, 0.05% Tween 20), blocked for 1 hour in TBSTw containing 5% milk (Sainsbury's powdered skimmed milk) and then incubated with primary antibody (1:500 or 1:1000) in TBSTw with 5% milk for 1 hour at room temperature or overnight at 4°C. HRP-conjugated secondary antibody (1:10,000 in TBSTw + 0.5% milk) was bound for 1 hour at room temperature.

Membranes were washed 2× 5 minutes, 1× 15 minutes and 2× 10 minutes following each antibody incubation. ECL reagents (Amersham Biosciences) were used for chemiluminescence detection, according to the manufacturer's instructions.

Immunofluorescence

Cultured cells (~1×10^4 to 5×10^5 cells/ml) were seeded overnight onto round coverslips (13 mm in diameter) in normal culture conditions. Unless otherwise noted, coverslips were rinsed once with Dulbecco's phosphate-buffered saline (D-PBS) followed by fixation with 4% paraformaldehyde for 3 minutes, washing for 2 minutes (D-PBS + 0.05% Triton X-100), permeabilization with D-PBS + 0.1% TX-100 D-PBS for 3 minutes, two washes for 2 minutes each, blocking in D-PBS + 3% BSA, two washes for 2 minutes each, followed by incubation with the primary antibody (rabbit polyclonal anti-invadolysin 1:250, mouse monoclonal anti-cortactin 1:500 in D-PBS + 0.3% BSA) for 1 hour at room temperature. Next the coverslips were washed 2× 2 minutes and incubated with the secondary antibody (Alexa Fluor 594 anti-mouse or anti-rabbit (1:500), Cy5 anti-rabbit (1:500), BODIPY (10 μg/ml) or 488 phalloidin (1:500) and DAPI (0.1 μg/ml) in D-PBS + 0.3% BSA). Finally the coverslips were washed 3× 2 minutes and mounted on glass slides with Mowiol-glycerol (Calbiochem). Cells were examined using an Olympus AX-70 Provis epifluorescence microscope, and images captured with a Hamamatsu Orca II CCD camera. Images were processed using SmartCapture 3 and Adobe Photoshop software.

Cells were stained for ADRP and TIP47 at 37°C as previously described (Ohsaki et al., 2005). In brief, cells were fixed with fresh 3% formaldehyde in 0.1 M phosphate buffer (pH 7.4) for 10 minutes for TIP47 staining, or cells were fixed for ADRP staining with 3% formaldehyde and 0.025% glutaraldehyde in 0.1 M phosphate buffer (pH 7.4) for 10 minutes. After fixation, cells were rinsed three times with D-PBS and permeabilized in D-PBS + 0.01% digitonin for 30 minutes. After permeabilization cells were rinsed with D-PBS and blocked with 3% BSA in D-PBS for 10 minutes, rinsed with D-PBS and stained with goat anti-ADRP (1:50, Santa Cruz, sc-32450) or guinea pig anti-TIP47 (1:100, Progen Biotechnik, GP30) for 30 minutes at 37°C in D-PBS + 0.3% BSA. Cells were then washed three times for 5 minutes before addition of the secondary antibodies [Alexa Fluor 594 anti-rabbit 1:500 (Molecular Probes-Invitrogen), Texas red anti-guinea pig 1:500 or Texas red anti-goat 1:500 (Jackson ImmunoResearch, West Grove, PA, USA)] and 10 μg/ml BODIPY 493/503, a neutral lipid dye (Molecular Probes-Invitrogen) and were then incubated for 30 minutes at 37°C. Finally coverslips were washed 4× 5 minutes in D-PBS (including DAPI at 0.1 μg/ml in the third wash) and cover slips were mounted and imaged as described above.

Antibody affinity purification

Polyclonal rabbit C-Ab2 antibody was affinity purified against the C-terminal fusion protein construct using a 1:1 mix of Affi-Gel 10 and Affi-Gel 15 activated affinity supports (Bio-Rad cat. no. 153-6098). Ni-NTA affinity purified fusion protein was firstly coupled to the Affi-Gel 10/15 combination in 100 mM MOPS (pH 7.5) overnight at 4°C, according to the manufacturer's recommendations. Following centrifugation and removal of the supernatant, the beads were incubated with 1 ml of 1 M ethanolamine (pH 8 with HCl) for 1 hour at 4°C to block any active esters. The resulting slurry was then transferred to Bio-Rad chromatography columns (Bio-Rad cat. no. 731-1550) and washed with 50 mM Tris-HCl (pH 8.8), followed by TBS (137 mM NaCl, 20 mM Tris-HCl, pH 7.6) and Tris high salt (500 mM NaCl, 20 mM Tris-HCl pH 7.5). The C-Ab2 serum was then applied to the column and C-Ab2 antibody was eluted in 0.5 mM glycine (pH 2.5).

Invadopodia matrix degradation assay

Coverslips were coated with FITC-gelatine as previously described (Baldassarre et al., 2006). FITC-gelatine was prepared by dissolving 2 mg/ml gelatine in 61 mM NaCl, 50 mM $Na_2B_4O_7$, pH 9.3, for 1 hour at 65°C. Gelatine was cooled to room temperature and FITC (1.8 mg/ml) was added and mixed for 2 hours in complete darkness. FITC-gelatine was dialyzed in 3 l PBS for 2 days with two or three buffer changes per day. Sucrose (2% w/v) was added to the mixture prior to aliquoting and storing at 4°C. Coverslips, sterilized in 70% ethanol, were tilted and coated with warmed FITC-gelatine, any excess was removed, and they were then dried. Coated coverslips were inverted onto ice-cold 0.5% glutaraldehyde in D-PBS for 15 minutes at 4°C, followed by three gentle washes with D-PBS at room temperature. Next they were incubated with sodium borohydride (5 mg/ml in D-PBS) for 3 minutes at room temperature, followed by gently washing three times with D-PBS and sterilizing in 70% ethanol for 5 minutes. Coverslips were then briefly air dried and rinsed in DMEM for 1 hour at 37°C. They were stored at 4°C in D-PBS until required. Cells were seeded onto coverslips for 24 hours with no inhibitor or 20 hours in the presence of 25 μM GM6001 followed by 4 hours with no inhibitor. Cells were fixed, stained and imaged as detailed above.

Endocytosis assay

Cells were seeded on round coverslips (13 mm in diameter) in 6-well dishes and grown under normal conditions overnight. The next day, cells were starved for 30 minutes in DMEM lacking fetal bovine serum. Cholera toxin B or transferrin (Molecular Probes) was added to the cells at a final concentration of 10 μg/ml in medium. The cells were incubated at 37°C for 5, 10 or 20 minutes and the dyes were rinsed off with D-PBS (five rinses). Cells were fixed in 4% paraformaldehyde and immunofluorescence was carried out as described above. Brefeldin A treatment was performed before immunostaining for invadolysin and caveolin. A375 cells were treated with 5 μg/ml brefeldin A for 3 hours. After treatment, cell were fixed and stained with invadolysin and caveolin 1 antibody (Zymed Laboratories, California).

Subcellular fractionation

A375 melanoma cells cultured in several 175 cm flasks were incubated for 2 days with 300 μM oleic acid (Sigma). Cells were removed with trypsin, washed in PBS and resuspended in hypotonic buffer containing 10 mM NaCl, 10 mM EDTA, 10 mM Tris-HCl (pH 7.4), 1 mM PMSF (phenylmethylsulphonyl fluoride), CLAP (chymostatin, leupeptin, antipain and pepstatin at a final concentration of 0.1 μg/ml of each) and aprotinin (Sigma, 1:100 dilution). After incubation for 10 minutes in ice-cold hypotonic buffer, cells were homogenized in a cooled European Molecular Biology Laboratory (EMBL) cell cracker with 10 strokes using a maximum clearance of 12 μm. Homogenization was confirmed by inspection under a microscope before centrifuging (1000 ***g***, 5 minutes) to pellet nuclei and any unlysed cells, which were then resuspended in an equal volume of hypotonic buffer. An equal volume of 80% sucrose in hypotonic buffer was added to the supernatant and 2 ml of this solution was placed in SW50.1 Beckman ultracentrifuge tubes before overlaying with ice-cold 20%, 10%, 5% and 0% sucrose in hypotonic buffer. The gradients were centrifuged in a SW 50.1 swing-out rotor and spun under vacuum in a Beckman L7 ultracentrifuge at 95,764 ***g*** (average) for 2 hours at 4°C. The uppermost fraction was then removed using a Beckman tube slicer and subsequent fractions were collected by pipetting from the top down. The protein content of fractions was measured using the Bradford assay (Bradford, 1976) and triglyceride levels were measured by spectrophotometry using the Infinity enzymatic assay (Thermo Electron).

Phenotypic analysis of mutant *Drosophila*

Flies were propagated on a cornflour-molasses medium supplemented with dry yeast at 25°C and 20-30% humidity with a 12 hour light/dark cycle. *Drosophila* larvae were cultured at 25°C for 93-113 hours before dissecting on a glass slide. The dissected fat body was then fixed for 20 minutes in 4% formaldehyde in D-PBS. The fat body was washed twice for 20 minutes with D-PBS before staining with Nile Red (1:10,000, Fluka Analytical) for 2 hours at room temperature. The stained fat body was mounted in 90% glycerol and imaged with OptiGrid Structured Illumination Microscopy (SIM) integrated with a Nikon TE2000 inverted microscope, which operates as a plug-in for Volocity (Improvision, Coventry, UK).

The triglyceride assay was performed based on previously described work (Grönke et al., 2003). Briefly, whole larvae were collected and placed in 500 μl of 0.05% Tween 20 and homogenised using a Polytron apparatus, followed by heat inactivation at 70°C for 5 minutes. The samples were centrifuged for 1 minute at 1166 ***g*** and 350 μl of the supernatant was transferred to a new vial and centrifuged for 3 minutes at 595 ***g***. Protein content was determined using the Bradford assay (Bradford, 1976) and triglyceride levels were measured by spectrophotometry using the Infinity enzymatic assay (Thermo Electron).

The authors would like to express their gratitude to Bill Earnshaw and Mike Cousin for interesting and relevant discussions, as well as to Paddy Hadoke, Damien Hudson and Heck lab members for feedback on the manuscript. We are grateful to Grant Sellar, Laura Machesky, David Melton, Bill Earnshaw, Jim Ross and Adriano Rossi for cell lines and cultures. Albert Pol (Barcelona) was extremely helpful in advising on the isolation of lipid droplets from cultured cells. Walid Maalouf and Sari Pennings provided assistance with OptiGrid Structured Illumination Microscopy. This work was supported by a Wellcome Trust University Award to M.M.S.H., a postdoctoral fellowship from Medical Research Scotland to K.M.M., and a Darwin Trust PhD studentship to S.G.R. Work with orang-utan cell lines was supported by EUPRIM-Net under the EU contract RII3-026155 of the 6th Framework Programme. Deposited in PMC for release after 6 months.

References

Accioly, M. T., Pacheco, P., Maya-Monteiro, C. M., Carrossini, N., Robbs, B. K., Oliveira, S. S., Kaufmann, C., Morgado-Diaz, J. A., Bozza, P. T. and Viola, J. P. (2008). Lipid bodies are reservoirs of cyclooxygenase-2 and sites of prostaglandin-E2 synthesis in colon cancer cells. *Cancer Res.* **68**, 1732-1740.

Aronoff, D. M., Canetti, C. and Peters-Golden, M. (2004). Prostaglandin E2 inhibits alveolar macrophage phagocytosis through an E-prostanoid 2 receptor-mediated increase in intracellular cyclic AMP. *J. Immunol.* **173**, 559-565.

Ayala, I., Baldassarre, M., Caldieri, G. and Buccione, R. (2006). Invadopodia: a guided tour. *Eur. J. Cell Biol.* **85**, 159-164.

Baldassarre, M., Pompeo, A., Beznoussenko, G., Castaldi, C., Cortellino, S., McNiven, M. A., Luini, A. and Buccione, R. (2003). Dynamin participates in focal extracellular matrix degradation by invasive cells. *Mol. Biol. Cell* **14**, 1074-1084.

Baldassarre, M., Ayala, I., Beznoussenko, G., Giacchetti, G., Machesky, L. M., Luini, A. and Buccione, R. (2006). Actin dynamics at sites of extracellular matrix degradation. *Eur. J. Cell Biol.* **85**, 1217-1231.
Birch, P. R., Rehmany, A. P., Pritchard, L., Kamoun, S. and Beynon, J. L. (2006). Trafficking arms: oomycete effectors enter host plant cells. *Trends Microbiol.* **14**, 8-11.
Bradford, M. M. (1976). A rapid and sensitive method for the quantitation of microgram quantities of protein utilizing the principle of protein-dye binding. *Anal. Biochem*. **72**, 248-254.
Brasaemle, D. L., Barber, T., Kimmel, A. R. and Londos, C. (1997). Post-translational regulation of perilipin expression: stabilization by stored intracellular neutral lipids. *J. Biol. Chem*. **272**, 9378-9387.
Cermelli, S., Guo, Y., Gross, S. P. and Welte, M. A. (2006). The lipid-droplet proteome reveals that droplets are a protein-storage depot. *Curr. Biol.* **16**, 1783-1795.
D'Avila, H., Maya-Monteiro, C. M. and Bozza, P. T. (2008). Lipid bodies in innate immune response to bacterial and parasite infections. *Int. Immunopharmacol*. **8**, 1308-1315.
Etges, R. (1992). Identification of a surface metalloproteinase on 13 species of Leishmania isolated from humans, *Crithidia fasciculata*, and *Herpetomonas samuelpessoai*. *Acta Trop*. **50**, 205-217.
Frangioni, J. V. and Neel, B. G. (1993). Solubilization and purification of enzymatically active glutathione S-transferase (pGEX) fusion proteins. *Anal. Biochem.* **210**, 179-187.
Fujimoto, T., Kogo, H., Ishiguro, K., Tauchi, K. and Nomura, R. (2001). Caveolin-2 is targeted to lipid droplets, a new "membrane domain" in the cell. *J. Cell Biol.* **152**, 1079-1085.
Fukui, Y., de Hostos, E., Yumura, S., Kitanishi-Yumura, T. and Inou. (1999). Architectural dynamics of F-actin in eupodia suggests their role in invasive locomotion in Dictyostelium. *Exp. Cell Res.* **249**, 33-45.
Gomis-Rüth, F. X. (2003). Structural aspects of the metzincin clan of metalloendopeptidases. *Mol. Biotechnol.* **24**, 157-202.
Gossot, O. and Geitmann, A. (2007). Pollen tube growth: coping with mechanical obstacles involves the cytoskeleton. *Planta* **226**, 405-416.
Grande-Garcia, A. and del Pozo, M. A. (2008). Caveolin-1 in cell polarization and directional migration. *Eur. J. Cell Biol.* **87**, 641-647.
Grönke, S., Beller, M., Fellert, S., Ramakrishnan, H., Jäckle, H. and Kühnlein, R. P. (2003). Control of fat storage by a *Drosophila* PAT domain protein. *Curr. Biol.* **13**, 603-606.
Ilgoutz, S. C. and McConville, M. J. (2001). Function and assembly of the *Leishmania* surface coat. *Int. J. Parasitol.* **31**, 899-908.
Ivens, A. C., Peacock, C. S., Worthey, E. A., Murphy, L., Aggarwal, G., Berriman, M., Sisk, E., Rajandream, M. A., Adlem, E., Aert, R. et al. (2005). The genome of the kinetoplastid parasite, *Leishmania major*. *Science* **309**, 436-442.
Kadereit, B., Kumar, P., Wang, W. J., Miranda, D., Snapp, E. L., Severina, N., Torregroza, I., Evans, T. and Silver, D. L. (2008). Evolutionarily conserved gene family important for fat storage. *Proc. Natl. Acad. Sci. USA* **105**, 94-99.
King, N., Westbrook, M. J., Young, S. L., Kuo, A., Abedin, M., Chapman, J., Fairclough, S., Hellsten, U., Isogai, Y., Letunic, I. et al. (2008). The genome of the choanoflagellate *Monosiga brevicollis* and the origin of metazoans. *Nature* **451**, 783-788.
Kinoshita, T., Fukuzawa, H., Shimada, T., Saito, T. and Matsuda, Y. (1992). Primary structure and expression of a gamete lytic enzyme in *Chlamydomonas reinhardtii*: similarity of functional domains to matrix metalloproteases. *Proc. Natl. Acad. Sci. USA* **89**, 4693-4697.
Li, L. C. and Cosgrove, D. J. (2001). Grass group I pollen allergens (beta-expansins) lack proteinase activity and do not cause wall loosening via proteolysis. *Eur. J. Biochem.* **268**, 4217-4226.
Linder, S. and Kopp, P. (2005). Podosomes at a glance. *J. Cell Sci.* **118**, 2079-2082.
López-Otín, C. and Overall, C. M. (2002). Protease degradomics: a new challenge for proteomics. *Nat. Rev. Mol. Cell Biol.* **3**, 509-519.
Marx, J. (2006). Cell biology: podosomes and invadopodia help mobile cells step lively. *Science* **312**, 1868-1869.
McConville, M. J. and Ferguson, M. A. (1993). The structure, biosynthesis and function of glycosylated phosphatidylinositols in the parasitic protozoa and higher eukaryotes. *Biochem. J.* **294**, 305-324.
McHugh, B., Krause, S. A., Yu, B., Deans, A. M., Heasman, S., McLaughlin, P. and Heck, M. M. (2004). Invadolysin: a novel, conserved metalloprotease links mitotic structural rearrangements with cell migration. *J. Cell Biol.* **167**, 673-686.
Miyanari, Y., Atsuzawa, K., Usuda, N., Watashi, K., Hishiki, T., Zayas, M., Bartenschlager, R., Wakita, T., Hijikata, M. and Shimotohno, K. (2007). The lipid droplet is an important organelle for hepatitis C virus production. *Nat. Cell Biol.* **9**, 1089-1097.
Murphy, D. J. (2001). The biogenesis and functions of lipid bodies in animals, plants and microorganisms. *Prog. Lipid Res.* **40**, 325-438.
Müller, G., Over, S., Wied, S. and Frick, W. (2008). Association of (c)AMP-degrading glycosylphosphatidylinositol-anchored proteins with lipid droplets is induced by palmitate, H_2O_2 and the sulfonylurea drug, glimepiride, in rat adipocytes. *Biochemistry* **47**, 1274-1287.
Naslavsky, N., Rahajeng, J., Rapaport, D., Horowitz, M. and Caplan, S. (2007). EHD1 regulates cholesterol homeostasis and lipid droplet storage. *Biochem. Biophys. Res. Commun.* **357**, 792-799.
Neurath, H. and Walsh, K. A. (1976). Role of proteolytic enzymes in biological regulation (a review). *Proc. Natl. Acad. Sci. USA* **73**, 3825-3832.
Notredame, C., Higgins, D. G. and Heringa, J. (2000). T-Coffee: A novel method for fast and accurate multiple sequence alignment. *J. Mol. Biol.* **302**, 205-217.
Ohsaki, Y., Maeda, T. and Fujimoto, T. (2005). Fixation and permeabilization protocol is critical for the immunolabeling of lipid droplet proteins. *Histochem. Cell Biol.* **124**, 445-452.
Ohsaki, Y., Cheng, J., Fujita, A., Tokumoto, T. and Fujimoto, T. (2006). Cytoplasmic lipid droplets are sites of convergence of proteasomal and autophagic degradation of apolipoprotein B. *Mol. Biol. Cell* **17**, 2674-2683.
Orlandi, P. A. and Fishman, P. H. (1998). Filipin-dependent inhibition of cholera toxin: evidence for toxin internalization and activation through caveolae-like domains. *J. Cell Biol.* **141**, 905-915.
Ostermeyer, A. G., Paci, J. M., Zeng, Y., Lublin, D. M., Munro, S. and Brown, D. A. (2001). Accumulation of caveolin in the endoplasmic reticulum redirects the protein to lipid storage droplets. *J. Cell Biol.* **152**, 1071-1078.
Pol, A., Martin, S., Fernandez, M. A., Ferguson, C., Carozzi, A., Luetterforst, R., Enrich, C. and Parton, R. G. (2004). Dynamic and regulated association of caveolin with lipid bodies: modulation of lipid body motility and function by a dominant negative mutant. *Mol. Biol. Cell* **15**, 99-110.
Rappoport, J. Z. and Simon, S. M. (2003). Real-time analysis of clathrin-mediated endocytosis during cell migration. *J. Cell Sci.* **116**, 847-855.
Rothberg, K. G., Heuser, J. E., Donzell, W. C., Ying, Y. S., Glenney, J. R. and Anderson, R. G. (1992). Caveolin, a protein component of caveolae membrane coats. *Cell* **68**, 673-682.
Scherzer, C. R. and Feany, M. B. (2004). Yeast genetics targets lipids in Parkinson's disease. *Trends Genet.* **20**, 273-277.
Schlagenhauf, E., Etges, R. and Metcalf, P. (1998). The crystal structure of the *Leishmania major* surface proteinase leishmanolysin (gp63). *Structure* **6**, 1035-1046.
Schlegel, A. and Stainier, D. Y. (2007). Lessons from "lower" organisms: what worms, flies, and zebrafish can teach us about human energy metabolism. *PLoS Genet.* **3**, e199.
Schmidt, H. A., Strimmer, K., Vingron, M. and von Haeseler, A. (2002). TREE-PUZZLE: maximum likelihood phylogenetic analysis using quartets and parallel computing. *Bioinformatics* **18**, 502-504.
Serezani, C. H., Chung, J., Ballinger, M. N., Moore, B. B., Aronoff, D. M. and Peters-Golden, M. (2007). Prostaglandin E2 suppresses bacterial killing in alveolar macrophages by inhibiting NADPH oxidase. *Am. J. Respir. Cell Mol. Biol.* **37**, 562-570.
Smirnova, E., Goldberg, E. B., Makarova, K. S., Lin, L., Brown, W. J. and Jackson, C. L. (2006). ATGL has a key role in lipid droplet/adiposome degradation in mammalian cells. *EMBO Rep.* **7**, 106-113.
Soding, J., Biegert, A. and Lupas, A. N. (2005). The HHpred interactive server for protein homology detection and structure prediction. *Nucleic Acids Res.* **33**, W244-W248.
Srivastava, M., Begovic, E., Chapman, J., Putnam, N. H., Hellsten, U., Kawashima, T., Kuo, A., Mitros, T., Salamov, A., Carpenter, M. L. et al. (2008). The *Trichoplax* genome and the nature of placozoans. *Nature* **454**, 955-960.
Targett-Adams, P., Chambers, D., Gledhill, S., Hope, R. G., Coy, J. F., Girod, A. and McLauchlan, J. (2003). Live cell analysis and targeting of the lipid droplet-binding adipocyte differentiation-related protein. *J. Biol. Chem.* **278**, 15998-16007.
Teixeira, L., Rabouille, C., Rorth, P., Ephrussi, A. and Vanzo, N. F. (2003). *Drosophila* Perilipin/ADRP homologue Lsd2 regulates lipid metabolism. *Mech. Dev.* **120**, 1071-1081.
Thiele, C. and Spandl, J. (2008). Cell biology of lipid droplets. *Curr. Opin. Cell Biol.* **20**, 378-385.
Thompson, J. D., Higgins, D. G. and Gibson, T. J. (1994). CLUSTAL W: improving the sensitivity of progressive multiple sequence alignment through sequence weighting, position-specific gap penalties and weight matrix choice. *Nucleic Acids Res.* **22**, 4673-4680.
van Manen, H. J., Kraan, Y. M., Roos, D. and Otto, C. (2005). Single-cell Raman and fluorescence microscopy reveal the association of lipid bodies with phagosomes in leukocytes. *Proc. Natl. Acad. Sci. USA* **102**, 10159-10164.
Waltermann, M. and Steinbuchel, A. (2005). Neutral lipid bodies in prokaryotes: recent insights into structure, formation, and relationship to eukaryotic lipid depots. *J. Bacteriol.* **187**, 3607-3619.
Welte, M. A. (2007). Proteins under new management: lipid droplets deliver. *Trends Cell Biol.* **17**, 363-369.
Whelan, S. and Goldman, N. (2001). A general empirical model of protein evolution derived from multiple protein families using a maximum-likelihood approach. *Mol. Biol. Evol.* **18**, 691-699.
Wolins, N. E., Brasaemle, D. L. and Bickel, P. E. (2006). A proposed model of fat packaging by exchangeable lipid droplet proteins. *FEBS Lett.* **580**, 5484-5491.
Yao, C., Donelson, J. E. and Wilson, M. E. (2003). The major surface protease (MSP or GP63) of *Leishmania* sp. Biosynthesis, regulation of expression, and function. *Mol. Biochem. Parasitol.* **132**, 1-16.
Yao, M., Huang, Y., Shioi, K., Hattori, K., Murakami, T., Nakaigawa, N., Kishida, T., Nagashima, Y. and Kubota, Y. (2007). Expression of adipose differentiation-related protein: a predictor of cancer-specific survival in clear cell renal carcinoma. *Clin. Cancer Res.* **13**, 152-160.
Zheng, N. and Gierasch, L. M. (1996). Signal sequences: the same yet different. *Cell* **86**, 849-852.

Journal of Cell Science